ADVANCED ENERGY MATERIALS
www.advenergymat.de

On the Origin of the Ideality Factor in Perovskite Solar Cells

Pietro Caprioglio, Christian M. Wolff, Oskar J. Sandberg, Ardalan Armin, Bernd Rech, Steve Albrecht, Dieter Neher,* and Martin Stolterfoht**

The measurement of the ideality factor (n_{id}) is a popular tool to infer the dominant recombination type in perovskite solar cells (PSC). However, the true meaning of its values is often misinterpreted in complex multilayered devices such as PSC. In this work, the effects of bulk and interface recombination on the n_{id} are investigated experimentally and theoretically. By coupling intensity-dependent quasi-Fermi level splitting measurements with drift diffusion simulations of complete devices and partial cell stacks, it is shown that interfacial recombination leads to a lower n_{id} compared to Shockley–Read–Hall (SRH) recombination in the bulk. As such, the strongest recombination channel determines the n_{id} of the complete cell. An analytical approach is used to rationalize that n_{id} values between 1 and 2 can originate exclusively from a single recombination process. By expanding the study over a wide range of the interfacial energy offsets and interfacial recombination velocities, it is shown that an ideality factor of nearly 1 is usually indicative of strong first-order nonradiative interface recombination and that it correlates with a lower device performance. It is only when interface recombination is largely suppressed and bulk SRH recombination dominates that a small n_{id} is again desirable.

1. Introduction

Halide perovskite solar cells (PSC) have the potential to trigger a revolution in the photovoltaic sector due to their low-cost production and outstanding efficiencies. The material combines exceptional properties such as a high absorption coefficient, panchromatic light absorption,[1] long carrier diffusion lengths,[2,3] shallow trap energy levels,[4] and astonishingly high (external) photoluminescence (PL) yields (up to 66%[5]), rendering its optoelectronic quality comparable to that of GaAs.[6] Generally, all these properties allow for a high photocurrent collection and low nonradiative recombination losses. However, despite the continuous advance of the scientific community in increasing the power conversion efficiencies (PCEs), perovskite solar cells are still limited by the open-circuit voltage (V_{OC}). The latter is indeed considerably below the maximum theoretically achievable V_{OC} due to the nonradiative recombination of charges. In order to fully exploit the thermodynamic potential of this material, a deeper understanding of these recombination processes has to be accomplished. Through the years, several studies spotlighted the perovskite surface[7–9] and the grain boundaries[9,10] as main recombination centers in the perovskite absorber. More recently, the perovskite/transport layer (TL) junctions have been identified as the main source of free energy losses in several efficient devices due to significant nonradiative recombination taking place across these internal interfaces.[11–14] However, only a few studies aimed at identifying the interplay and the relative importance of the recombination losses in the perovskite bulk, at the interfaces and/or at the metal contacts.[15–20] One of the most popular approaches to assess the dominant recombination mechanism is the measurement of the ideality factor (n_{id}).[17,18,21–23] This figure of merit describes the deviation from the ideal diode behavior where only bimolecular recombination is considered as recombination process. An elegant and already well-established approach to determine the n_{id} is to measure the V_{OC} as a function of the light intensity (I). This avoids the issue of poor transport properties and related voltage losses which become problematic when extracting the n_{id} from dark current–voltage characteristics.[23,24] Commonly, $n_{id} = 1$ is assumed to be representative of a second-order (bimolecular) radiative recombination of free charges, whereas $n_{id} = 2$ is attributed to a first-order (monomolecular) nonradiative recombination process, e.g., trap-assisted recombination through

P. Caprioglio, C. M. Wolff, Prof. D. Neher, Dr. M. Stolterfoht
Institute of Physics and Astronomy
University of Potsdam
Potsdam 14476, Germany
E-mail: capriogl@uni-potsdam.de; neher@uni-potsdam.de; stolterf@uni-potsdam.de

P. Caprioglio, Prof. S. Albrecht
Young Investigator Group Perovskite Tandem Solar Cells
Helmholtz-Zentrum Berlin für Materialien und Energie GmbH
Berlin 12489, Germany

Dr. O. J. Sandberg, Dr. A. Armin
Department of Physics
Swansea University
Singleton Park, Swansea, Wales SA2 8PP, UK

Prof. B. Rech
Institute for Silicon Photovoltaics
Helmholtz-Zentrum Berlin für Materialien und Energie GmbH
Berlin 12489, Germany

Prof. B. Rech, Prof. S. Albrecht
Faculty IV – Electrical Engineering and Computer Science Technical University Berlin
Berlin 10587, Germany

The ORCID identification number(s) for the author(s) of this article can be found under https://doi.org/10.1002/aenm.202000502.

DOI: 10.1002/aenm.202000502

mid-gap trap states.[25,26] In this picture, reported values of the n_{id} between 1 and 2 in efficient perovskite solar cells suggest a superposition of first- and second-order recombination, where the value of n_{id} depends on the relative strength of one or the other process. However, this often used approach to connect the value of the ideality factor to the order of recombination relies on several critical assumptions. The first one is that the very same carrier reservoir determines all recombination processes, meaning that the recombination current, J_R, can be written as $J_R \propto k_1 n + k_2 n^2 + k_3 n^3 \cong k_\alpha n^\alpha$, where α is the effective recombination order at the respective carrier density n, in the case equal electron and hole density. The second assumption concerns the relation between n and the external voltage (V), which is assumed to follow an exponential dependence $n \propto e^{\left(\frac{qV}{\vartheta k_B T}\right)}$, where ϑ is a parameter describing the density of state distribution at the bandedge,[27,28] $k_B T$ is the thermal energy, and q is the elementary charge. This approximation, however, requires that the electron density is proportional to the hole density at the dominant recombination site ($n_e \propto n_h \propto n$). Only then, the ideality factor is related to the recombination order via the well-known relation $n_{id} = \vartheta/\alpha$. None of these conditions are fulfilled in perovskite solar cells.

As pointed out above, the recombination under a 1 sun equivalent illumination intensity in *p-i-n*-type perovskite solar cells is mainly a first-order non-radiative trap-assisted process at the perovskite/TL interfaces. Radiative second-order recombination, on the other hand, is believed to originate strictly from the perovskite absorber, as there is no evidence for additional interfacial radiative recombination in the electroluminescence and PL emission spectra of the complete devices. Therefore, it is likely that first- and second-order recombination processes are controlled by different carrier reservoirs. Second, a strong interface recombination would drive a current of electrons and holes toward the respective TL even at V_{OC}, potentially causing the V_{OC} to be smaller than the quasi-Fermi level splitting (QFLS) in the perovskite bulk. Consequently, analyzing the total recombination current as function of V_{OC} may lead to wrong conclusions about mechanism of the recombination in the absorber and at its interfaces to the TLs.[15,16] We have recently measured the intensity dependence of the QFLS and the V_{OC} of complete perovskite solar cells for two different polymer-based hole transporting materials.[16] That work showed how interface recombination and energetic offsets cause a significant deviation of the device V_{OC} from the perovskite QFLS. We found the ideality factor of devices using poly[bis(4-phenyl)(2,4,6-trimethylphenyl)amine] (PTAA) as hole-transporting layer (HTL) to be around 1.3, which we could consistently attribute to trap-assisted recombination regardless of involving radiative second-order recombination. Another process affecting the ideality factor is the recombination at the metal contacts, which may lead to a saturation of the V_{OC} despite increasing the carrier density in the bulk, resulting in n_{id} approaching a value of 1 (or even decreasing below unity) at high intensities (typically above 1 sun). Nevertheless, only a few successful attempts to interpret and address the origin and the wide spread of the n_{id} values in perovskite solar cells have been reported in literature.[12,22,28,29]

Here, we extend our previous studies by utilizing intensity dependent PL measurements on perovskite films with and without transport layers in order to obtain the internal n_{id} (from QFLS) of the individual junctions of the cell and the neat material and to rationalize the origin of the n_{id} values previously observed.[16,17] This allows us to study the impact of a particular interface on the n_{id} with the aim to ultimately understand which recombination mechanism controls its value in the full cell. In particular, we find that the perovskite/C_{60} junction and the complete device exhibit an almost identical ideality factor, which suggests that this interface governs the ideality factor of the cell. On the other hand, despite an overall higher QFLS, a passivated neat perovskite film presents a higher n_{id} value due to reduced surface recombination.[30] By corroborating our results by drift diffusion simulations, we clarify that a single non-radiative recombination process at the interface can cause such *mixed* (between 1 and 2) n_{id} values. Furthermore, we study the impact of a broader range of parameters on the n_{id}, such as the interface recombination velocity and the majority carrier band offset. With that, we thoroughly explain, experimentally and theoretically, that a low ideality factor in many cases correlates to low V_{OC}s and poor device performances. Based on an analytical model, we then explain how Shockley–Read–Hall (SRH) recombination at the perovskite/TL interface accounts for the rather low n_{id} of all devices in this study. In this picture, the ideality factor of the cell depends essentially on the asymmetry of the electron and hole quasi-Fermi levels at the dominant recombination site. As previously observed empirically,[22,31] here we rationalize how in interface limited solar cells, $n_{id} = 1$ is not a result of bimolecular recombination of free charge carriers and does not necessarily correspond to a better performing device, as often assumed.

2. Results

Our combined experimental/simulation study focusses on *p-i-n* type "triple cation" perovskite solar cells, where the ≈450 nm thick perovskite absorber is sandwiched between a ≈10 nm thick HTL polymer and 30 nm thick electron-transporting layer (ETL).[32] Our state-of-the-art *p-i-n*-type cells include neat (undoped) PTAA as the HTL and neat C_{60} as the ETL.[7] The nominal composition of the perovskite absorber is $(Cs_{0.05}(MA_{0.17}FA_{0.83})_{0.95})Pb(I_{0.83}Br_{0.17})_3$, with an optical bandgap of 1.62 eV.[32] Indium-doped tin oxide (ITO) and Cu are used as the bottom anode and the top cathode, respectively. In this configuration, the devices regularly exhibit PCEs around 20% and they are characterized by V_{OC}s of 1.14 V and FFs of 78%.[13,16] Figure S1 in the Supporting Information displays *JV*-characteristics measured in forward and reverse direction with different scan speeds. The comparatively small hysteresis at different scan rates suggests only a minor effect of the ion motion on the device characteristics under operational conditions. As shown in our previous work, recombination in such devices is determined by non-radiative interfacial recombination, which limits the photoluminescence quantum yield (PLQY) to values well below 1%. Despite the insignificance of radiative recombination in the bulk, these devices have ideality factors of ≈1.3. If n_{id} would be entirely determined by the competition between

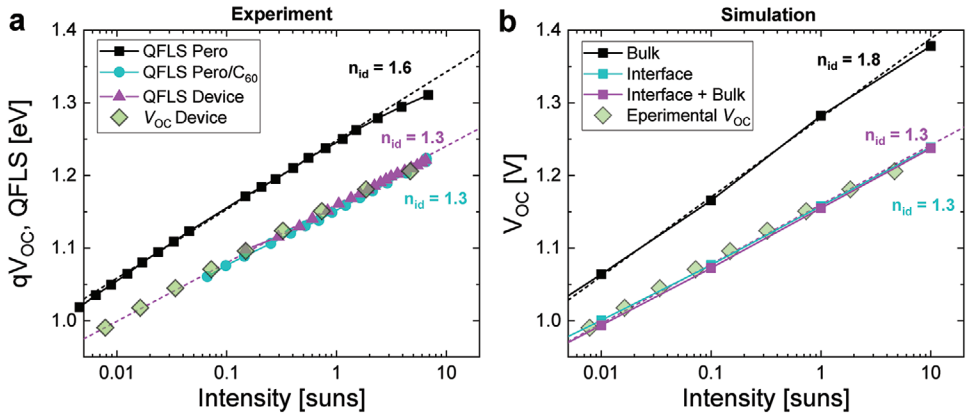

Figure 1. a) Intensity dependent quasi-Fermi level splitting, QFLS(I), of a neat TOPO-passivated perovskite, a perovskite/C_{60} bilayer, and a complete device structure (including electrodes) in addition to the intensity dependent V_{OC} of the device. Dashed lines show fits to an exponential dependence on the illumination intensity, yielding the internal ideality factor. b) $V_{OC}(I)$ as obtained from drift-diffusion simulations of a typical perovskite solar cell utilizing PTAA and C_{60} as HTL and ETL, respectively. The results show the effects of different recombination types on the ideality factor. The ideality factor is largest when only radiative and non-radiative bulk recombination is considered (black) as compared to the case of interface recombination only (turquoise) or a combination of interface and bulk recombination (magenta), in good agreement to the experimental results.

non-radiative first-order and radiative second-order recombination of the same carrier reservoir (see Section S5, Supporting Information, for derivation), then

$$n_{id} = \frac{2}{(1+\mathrm{PLQY})} \quad (1)$$

Note that PLQY will generally differ from the internal PL quantum efficiency by the outcoupling efficiency and parasitic losses.[33,34] For the considered cells, the PLQY is ≈0.1%. In this case, Equation (1) predicts $n_{id} \cong 2$, which is well above the measured value. Therefore, this shows that radiative recombination cannot be responsible for the ideality factor in our devices (≈1.3). To show how different parts of the device determine the value of n_{id}, we performed intensity dependent PL measurements on different layer combinations, including the neat surface-passivated perovskite absorber, different perovskite/transport layer junctions (perovskite/ETL, perovskite/HTL) and the complete device. The neat perovskite is surface-passivated with trioctylphosphine oxide (TOPO)[6,35] in order to probe mainly the recombination in the perovskite bulk (PLQY ≈5% under 1 sun conditions). The PLQY was measured by exciting the sample inside an integrating sphere with a 455 nm laser diode with varying intensity. In order to avoid possible effects induced by the illumination exposure time, all measurements have been performed under the exact same conditions with illumination time of ≈1 s for each point. In this regard, it has been noted that transient effects could influence the determination of n_{id} from $V_{OC}(I)$ measurements.[18] We, therefore, performed measurement of the PLQY and V_{OC} as function of illumination intensity with different exposure times (see Figure S2, Supporting Information). No significant variation was found within the timeframe studied here, confirming the robustness of our results and their relevance for operational conditions. From these results, the QFLS in the perovskite absorber was calculated at each intensity, following the approach as outlined in our previous works[16] (see also Figure S3, Supporting Information, for further details). Note that the QFLS of the complete device was measured at open circuit conditions. Finally, we, determined the internal and external ideality factor by fitting QFLS(I) and $V_{OC}(I)$, respectively, to an exponential dependence $J_R(I) = J_0 \cdot e^{\left(\frac{\mathrm{QFLS}(I)}{n_{id,int} k_B T}\right)}$ and $J_R(I) = J_0 \cdot e^{\left(\frac{qV_{OC}(I)}{n_{id,ext} k_B T}\right)}$. Here, $J_R(I)$ is the intensity dependent recombination current density, which is equal to the generation current density at V_{OC} and J_0 is the dark saturation current density.

The results are shown in **Figure 1**a, together with the intensity dependent V_{OC} of the device. In agreement with previous results, for the complete device, the fit of the intensity dependent QFLS yields $n_{id,int} \approx 1.3$. Surprisingly, this value is nearly identical to the value of $n_{id,ext} \approx 1.3$ as deduced from the intensity dependence of the V_{OC}, provided that leakage through the thin PTAA layer can be avoided.[16] Notably, the neat TOPO passivated perovskite has a $n_{id} \approx 1.6$, which is significantly larger than that of the full device. However, when the C_{60} layer is attached to the perovskite (on glass), the n_{id} value drops to roughly 1.3; the same value as of the complete cell. We have recently shown that the performance of such PTAA/perovskite/C_{60} *p-i-n*-type cells is dominated by non-radiative recombination at the perovskite/ETL interface.[13,15] Therefore, we conclude that 1) interfacial recombination leads to lower n_{id} compared to the recombination in the bulk and 2) the recombination at the least optimum interface (here the perovskite/C_{60} interface) determines the ideality factor of the complete cell. Importantly, for this type of devices, the internal QFLS and external V_{OC} match within the light intensity regime studied here. Lastly, we note that the non-passivated perovskite lies in between with $n_{id} = 1.45$ (Figure S4, Supporting Information). This suggests that the recombination at the perovskite surface results in a similar n_{id} as the C_{60} interface.

To confirm this experimental insight, we performed drift-diffusion simulations using our previously established simulation model.[15,16] All simulation parameters are listed in Table S1 in the Supporting Information. Importantly, the values of the interface recombination velocities and bulk lifetimes were determined from transient photoluminescence while the

energy offsets at the HTL/perovskite interfaces were measured with ultraviolet photoemission spectroscopy.[13,15] The values for the carrier mobilities in the different layers were optimized by fitting the *JV*-curves of samples with different layer thicknesses. The corresponding data and simulation results are shown in Figure S5 in the Supporting Information. The resulting *JV*-curve and the voltage dependent recombination losses (in the bulk, interface, contacts, etc.) corresponding to our standard settings are shown in Figure S6 in the Supporting Information. Although the simulation tool used here does not include ion motion in the absorber layer, given the excellent match of the simulations with a large number of different experiments and the absence hysteresis in our device, we believe that for the particular systems studied here, using fullerenes as ETL, the ion movement is not a decisive parameter, consistent with previous reports.[36] Overall, the simulations can well reproduce the intensity dependence of the V_{OC} of our cells as shown in Figure 1b. Moreover, the ideality factor of the device is identical (≈1.3) regardless whether recombination in perovskite bulk (both radiative and SRH) is implemented or not. In contrast, if we consider only bulk recombination (device with ideal interfaces), then the ideality factor is considerably higher (≈1.8). Here, we implemented a SRH lifetime of 1 µs (for the passivated perovskite) and a k_2 of 6×10^{-11} cm^3 s^{-1} [37] (see Section S5, Supporting Information, for other settings). Importantly, as expected from Equation (1), k_2 has a certain impact on the ideality factor at high intensities, above 1 sun, when the PLQY becomes significantly large (Figure S7, Supporting Information). It is also important to note that the constant slope of the QFLS versus I in the case of the complete device and the perovskite/C_{60} bilayer suggests that n_{id} is dominated by a single recombination process (within the studied intensity regime). This indicates that n_{id} values between 1 and 2 do not originate from a competition of different recombination mechanisms, which would rather result in a change of slope when a different recombination mechanism takes over. We also note that in the neat passivated perovskite, we observe a bending of the QFLS at high intensities (10 suns), where bimolecular recombination is presumably starting to be the predominant recombination mechanism. Importantly, we have previously ruled out that heating is a determinant factor in causing this deviation at high intensities.[16]

Considering the relevance of the perovskite/TL interface in determining n_{id}, we performed simulations for a wide range of interfacial recombination velocities (S) and majority carrier band offsets (E_{maj}) at the HTL/perovskite interface. Note that from here on we will discuss the impact of these parameters on the external n_{id}. This was inspired by previous works which revealed a large effect of these parameters on the V_{OC} of *p-i-n* devices.[15,16] We kept an S of 2000 cm s^{-1} with no energy offset at the *n*-interface, while the injection barrier at the metal at both sides was kept constant. In **Figure 2**, we plot the ideality factor (Figure 2a) and the device V_{OC} (Figure 2b) versus S and E_{maj}. Several findings are important. First, the ideality factor drops rapidly to 1 (or even below) when increasing the majority carrier band-offset (the blue region in Figure 2a) even for small surface recombination velocities, while the drop of V_{OC} is more continuous. This reminds of the situation of dominant surface recombination.[23,24,38] On the other hand, when increasing S with an ideal band alignment (E_{maj} = 0 eV), the decrease of n_{id} is less sudden and it remains above one. Finally, its only for $E_{maj} \leq 0.1$ eV and $S < 1000$ cm s^{-1} that $n_{id} \approx 1.3$–1.4, consistent with our experimental data. Importantly, none of the input parameters yields $n_{id} = 2$, as it would have been predicted for predominant trap-assisted recombination by the simple model introduced above. In contrast, reducing the quality of the perovskite/TL interface decreases the value of n_{id} (along with a decrease of the V_{OC}), irrespectively of whether E_{maj}, S or both of them are increased. Therefore, in most cases a small n_{id} indicates the presence of a nonideal interface rather than predominant radiative recombination. In other words, the plot shows that an n_{id} of 1 is not necessarily representing an efficient cell as often believed (and suggested in other works).[39,40]

In order to provide further insights into the origin of these ideality factor values, we analyzed the hole (n_h) and electron (n_e) densities at the spatial location in the device where most of the recombination happens. Notably, the recombination rate at this location sets the upper limit for the V_{OC} at a given intensity and therefore defines the ideality factor. Given that the PLQY of all of our devices is below 1%, we consider only trap mediated

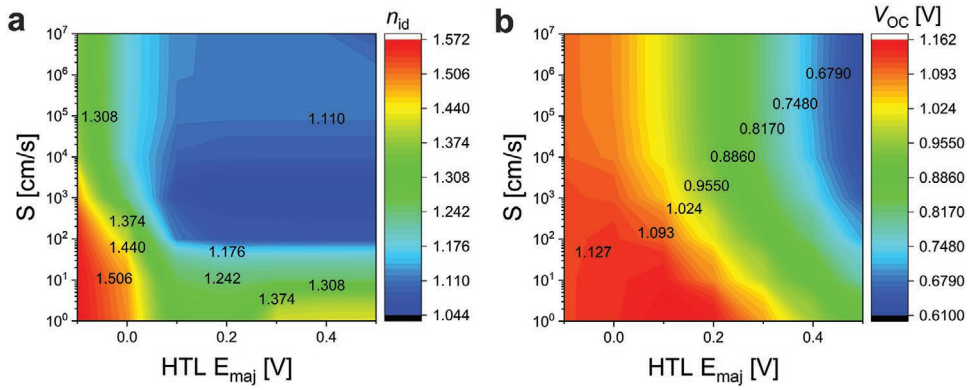

Figure 2. a) Numerically simulated external n_{id} and open-circuit voltages b) as a function of the interface recombination velocity S and the majority carrier band offset (E_{maj}) for holes at the HTL/perovskite interface. The blue area in panel (a) shows a region with strong interfacial recombination which results in an ideality factor of 1 and b) a low device V_{OC}. In contrast, weaker interface recombination (small energetic offsets and low S) cause an ideality factor of ≈1.3–1.4 as observed in our optimized cells.

recombination in the bulk and/or at the interfaces. In the case of imbalanced carrier densities (e.g., $n_e \ll n_h$) and mid-gap trap states (with negligible detrapping), the recombination rate will be almost entirely determined by the minority carrier density (e.g., electrons) (extended derivation in Section S7, Supporting Information). Then, the recombination rate can be written in terms of the QFLS at the location of predominant recombination as follows

$$R_{SRH}(I) \propto n_{min}(I) \propto e^{\left(\frac{E_{F,min}(I)-E_F^0}{k_BT}\right)} \propto e^{\left(\frac{\Delta E_{F,min}(I)}{k_BT}\right)} \propto e^{\left(\frac{\theta \times QFLS(I)}{k_BT}\right)} \propto e^{\left(\frac{QFLS(I)}{n_{id}k_BT}\right)} \quad (2)$$

where $n_{min}(I)$ is the intensity dependent density of the minority carriers at the recombination site, $E_{F,min}$ is the quasi-Fermi level of the minority carriers, E_F^0 is the intrinsic Fermi level in the dark, and $\theta \times QFLS(I)$ is the minority carriers share of the total QFLS increase when increasing I. According to Equation (2), this situation leads to

$$n_{id} = \frac{1}{\theta} \quad (3)$$

In other words, the value of n_{id} is given by the share of the QFLS that $E_{F,min}$ gets when the QFLS increases as function of light intensity. In the extreme case, where the majority carrier density is fixed and the increase of the QFLS is only due to the increase of the minority carriers, the ideality factor is 1 despite the fact that all recombination is due to first order non-radiative processes (see Section S7, Supporting Information, for derivation). On the other hand, when n_e and n_h at the dominant recombination site are nearly equal (for example, when the recombination happens in the bulk or in case of a near-ideal interface),the quasi-Fermi levels for electron and holes ($E_{F,e}$ and $E_{F,h}$) would share the total QFLS symmetrically, resulting in an n_{id} of 2. **Figure 3** visually depicts the scenarios of the two cases described above. Note that interface recombination may cause a significant bending of the majority quasi-Fermi levels in the perovskite bulk ($E_{F,e}$ at the ETL and $E_{F,h}$ at the HTL), which has its origin in the depletion of the majority carrier density in the perovskite near the TL due to a large energy offset in combination with fast surface recombination. Therefore, the measured V_{OC} will not necessarily be equal to the QFLS at the dominant recombination side; however, this is considered in the model. The situation becomes less complicated if this band bending exists only at one of the interfaces and if this is the interface of predominant recombination. The reason is that qV_{OC} is the difference between the Fermi levels at the two contacts, which in this special case, is identical to the QFLS at the dominant recombination region.

Numerical simulations and V_{OC} versus I experiments of systems with different n_{id} are exemplified in **Figure 4**a. For these systems, in Figure 4b–e, we plot the simulated n_h (n_e) and $E_{F,e}$ ($E_{F,h}$) at the site of predominant recombination as function of intensity and V_{OC}, respectively, in order to visualize the symmetry of the QFLS and to corroborate the validity of our approach to explain the simulated and experimentally determined n_{id}. This is shown for perovskite solar cells with various HTLs characterized by different majority carrier energetic offsets and interface recombination at the *p*-interface. These HTLs include undoped poly(3-hexylthiophene) (P3HT) ($E_{maj} \approx 0.2$ eV) and doped poly(3,4-ethylenedioxythiophene) polystyrene sulfonate (PEDOT:PSS) ($E_{maj} \approx 0.4$ eV).[15,16] Consistent with earlier studies, both types of devices show ideality factors approaching 1 and low V_{OC}s.[12,20] Importantly, given the large energetic offset and the strong interface recombination, these two systems exhibit a significant mismatch between the QFLS in the bulk and the V_{OC}. However, in case of predominant recombination at the perovskite/TL interface, the QLFS in the perovskite is irrelevant for the interfacial recombination rate as the recombination rate is determined by the difference of the electron and hole quasi-Fermi levels at the HTL interface. In case of only one dominant interface this QFLS is then equal to the V_{OC} (see Figure 3 and Figure S8A, Supporting Information).

For all cases, we obtain θ from the intensity dependence of $\Delta E_{F,min}(I) \propto \theta \times QFLS(I)$, where θ is the slope representing the minority carrier share of the QFLS increase. In the case of the ideal device, most of the recombination happens in the bulk. Due to the lack of interface recombination ($S = 0$), n_e and n_h are

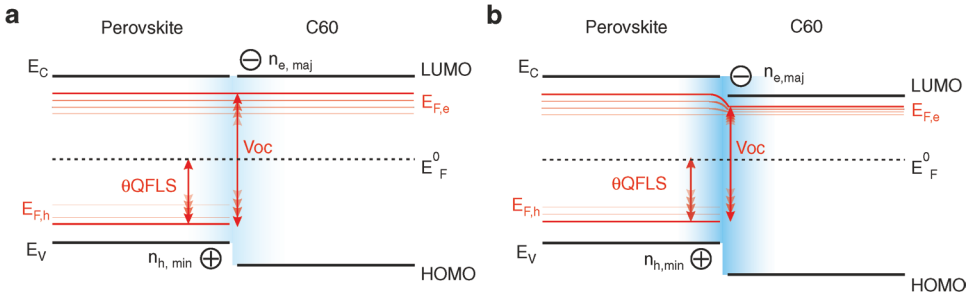

Figure 3. Schemes of interfacial energy levels and quasi-Fermi level splitting (QFLS) based on a simulated energy diagram. Importantly, this picture only represents the situation in close proximity to the interface and we acknowledge that inside the individual layers additional space charge effects might be present influencing the internal electric field. a) Exemplified scenario with negligible interface recombination and perfect energy alignment. Here, the electron (n_e) and hole carrier densities (n_h) are balanced and the splitting of the quasi-Fermi levels is symmetric. In this case, the hole quasi-Fermi level share of the total QFLS increase is 0.5. According to Equation (3), this results in $n_{id} = 1/\theta = 2$, in the case of dominant SRH recombination through mid-gap states. Notably, we still refer to holes as minority carriers for consistency with Equation (3), although in this case n_e and n_h are equal. b) Exemplified scenario with fast interface recombination and energetic offset. Here, the electron and hole carrier densities are unbalanced and the splitting of the quasi-Fermi levels is asymmetric. This scenario would give an n_{id} close to 1 because the QFLS increase is mostly due to the increase of the hole quasi-Fermi level (minority carriers) and therefore, θ is close to 1.

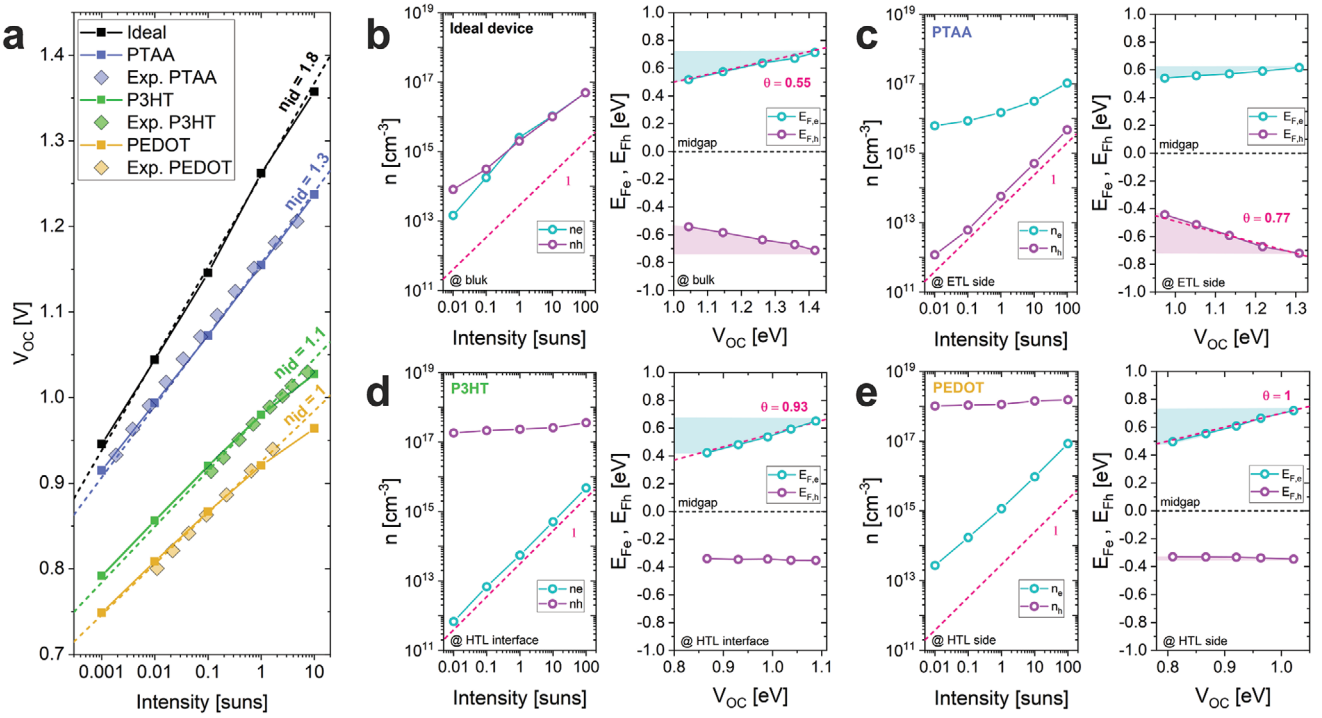

Figure 4. a) V_{OC} versus intensity obtained from experimental and numerical simulations of perovskite solar cells utilizing PTAA. P3HT, and PEDOT:PSS as hole transport layer (HTL) and C_{60} as electron transport layer (ETL), respectively. We note that while the PEDOT:PSS is slightly thicker (≈20 nm), the P3HT layer has the same thickness as PTAA. In black, a simulated cell with PTAA without interfacial recombination. In purple, simulation and experimental results of our reference cell with PTAA with realistic interface recombination. In green, simulation and experimental results for the P3HT cell considering a misaligned highest occupied molecular orbital with respect to the perovskite valence band (E_{maj} = 0.2 eV). In yellow, simulation and experimental results for a cell with a highly *p*-doped (10^{18} cm^{-3}) PEDOT:PSS layers and E_{maj} = 0.4 eV. The red line corresponds to a simulation with the standard settings but misaligned energy levels at the HTL-interface (E_{maj} = 0.5 eV). b–e) The left panels show the electron and holes densities as a function of the light intensity for each of the systems shown in (a). The dashed magenda line indicates a linear dependence of carrier density with respect to the light intensity. The right panels show the electron and hole quasi-Fermi levels at the site of predominant recombination, plotted against the respective V_{OC} of the cell. The series shows how in devices with a large majority carrier energy level offset and faster interface recombination, the majority carrier density in the TL is essentially pinned while the minority carrier density increases linearly with the intensity. This scenario results in an asymmetry of the splitting quasi-Fermi levels. The band diagram of the two extreme cases (b) and (e) is represented schematically in Figure 3.

nearly equal and the QFLS splits almost completely symmetrically with respect to the light intensity. In this case, the internal QFLS in the bulk is equal to the external V_{OC}, resulting in n_{id} of nearly two. In contrast, in the standard PTAA/perovskite/C_{60} cell with no energy offset on both sides, S_h = 200 cm s^{-1} and S_e = 2000 cm s^{-1}, we find that $n_e > n_h$ at the ETL interface and therefore the recombination rate depends mostly on n_h. Importantly, both n_e and n_h depend on the illumination intensity, yet the dependence of n_e is weaker. The reason is that electron injection from the cathode leads to a constant background electron density in the ETL (remote doping). On the other hand, because of the negligible energy offset to the perovskite conduction band, there exists a quasi-equilibrium between electrons in the ETL and in the perovskite, with the electron density in the latter being a function of intensity. Moreover, fast interface recombination at this interface induces a slower increase of n_e in the ETL layer compared to the perovskite bulk. Overall, this can explain the rather small increase of $n_e(I)$ in the ETL and as a consequence, the ratio θ at which $E_{F,min}$ increases with respect to the increase of the total QFLS with the light intensity, is 0.77 and equivalent to n_{id} = 1.3. In the extreme case of a cell with PEDOT:PSS, the strong *p*-doping of the HTL in combination with a large majority carrier band offset causes the carrier concentration to be highly unbalanced ($n_h \gg n_e$) at the perovskite/HTL interface, but also n_h to be constant within the intensity range studied. Thus, the recombination rate is completely governed by n_e and consequently, θ = 1 and n_{id} = 1. Also in the case of P3HT, which is characterized by a more moderate energetic offset and no doping, the model reconstructs precisely the experimentally determined n_{id}. Interestingly, also in a hypothetical solar cell with a strongly misaligned (but undoped) PTAA layer (Figure S8B, Supporting Information), the situation is almost identical to PEDOT:PSS, suggesting a stronger influence of the energetic offset on the n_{id} rather than doping. One reason is that the large energy offset in combination with interface recombination prevents that holes in the HTL exhibit a quasi-equilibrium with holes in the perovskite, meaning that n_h in the HTL becomes nearly independent of illumination intensity. All the obtained values are reported in **Table 1**.

Importantly, in all cases with interface recombination, the minority carrier density increases linearly with illumination intensity, meaning that its density at the contact is governed by a first order recombination process. Yet, the ideality factor is close or equal to 1. Therefore, n_{id} = 1 must not be misinterpreted

Table 1. Summary of V_{OC}, n_{id} from *JV*-scans, θ, and n_{id} calculated from θ for the ideal device, the PTAA device, the PEDOT:PSS device, and the PTAA device with an energetic offset.

	V_{OC} [V]	n_{id}	θ	n_{id} (θ)
Ideal device	1.26	1.8	0.55	1.81
PTAA	1.13	1.3	0.77	1.29
P3HT	0.96	1.1	0.93	1.07
PEDOT:PSS	0.87	1	1	1
PTAA (0.5 eV offset)	0.75	1	1	1

as radiative bimolecular recombination of free carriers, as often wrongly assumed. Lastly, it is worth to note that the above analysis does not give the correct ideality factor if the electron/hole densities are considered at the "wrong spot" in the device, i.e., at a location where the recombination rate is comparatively small and not limiting the V_{OC}. This is shown in Figure S9 in the Supporting Information for the PTAA device, where the same analysis is done using the carrier densities in the bulk, which results in $n_{id} = 1.8$ as expected for SRH in the bulk of our cells. Notably, the strength of the recombination at the metal contacts does not influence the above discussed recombination picture, as shown in Figure S10 in the Supporting Information.

Consequently, and to some extent counterintuitively, a higher n_{id} may actually correspond to a better perovskite device. These conclusions are summarized in **Figure 5**a,b, where we show the simulated n_{id} values of a perovskite solar cell by reducing first the energetic offset at the HTL interface (E_{maj}), then interface recombination and finally the contribution of bulk SRH over bimolecular recombination. In Figure 5b, experimental data points of devices with different degree of interface recombination and E_{maj} are included. The respective *JV*-characteristic of all devices are presented in Figure S11 in the Supporting Information, while the n_{id} of the LiF passivated cell with a PCE of ≈21% is shown in Figure S12 in the Supporting Information. It is evident that a larger n_{id} corresponds to larger V_{OC} in the interface limited region, while the trend is opposite in the bulk limited regime. This trend is confirmed experimentally by the series of devices with higher V_{OC}s and higher n_{id}. It is only in the case of optimized interfaces and highly suppressed interface recombination that an n_{id} of 1 would be again desirable, being representative of predominant free carrier recombination and reduced SRH in the bulk. However, we emphasize that we cannot exclude that other parameters may affect this trend in other devices.[41] Consistent with our experiments (passivated neat perovskite film, Figure 1a), in the bulk limited regime in Figure 5a), we observe a transition from a bulk SRH dominated to a bimolecular dominated n_{id} when going from low to high intensity. On the contrary, in the interface limited region, no interplay between different recombination processes is observed. Interestingly, in the bulk limited regime, the ideality factor as a function of V_{OC} changes faster than in the interfaces limited region when approaching the Shockley–Queisser (SQ) limit. On the other hand, especially for V_{OC}s below 1.2 V, the variation in n_{id} with respect to the V_{OC} increase is rather small.

3. Conclusions

In this work, we demonstrated the application of intensity dependent QFLS measurements on perovskite/transport layer junctions to gain a comprehensive understanding of the processes determining the ideality factor in perovskite solar cells. Through experiments and numerical simulations, we found that the ideality factor of ≈1.3 in our efficient perovskite cells (≈20% PCE) is a direct consequence of interfacial recombination at the C_{60} interface and is not a result of the interplay between SRH and bimolecular recombination in the absorber layer. Moreover, we demonstrated that increased interfacial recombination reduces the ideality factor towards 1 in the case of cells with a PEDOT:PSS and P3HT HTL. In order to delineate a more general picture, we studied the effects of energy misalignment and interface recombination on the n_{id} and V_{OC}. From these results, we show that for the device parameters studied herein, an n_{id} = 1 corresponds to a very unfavorable

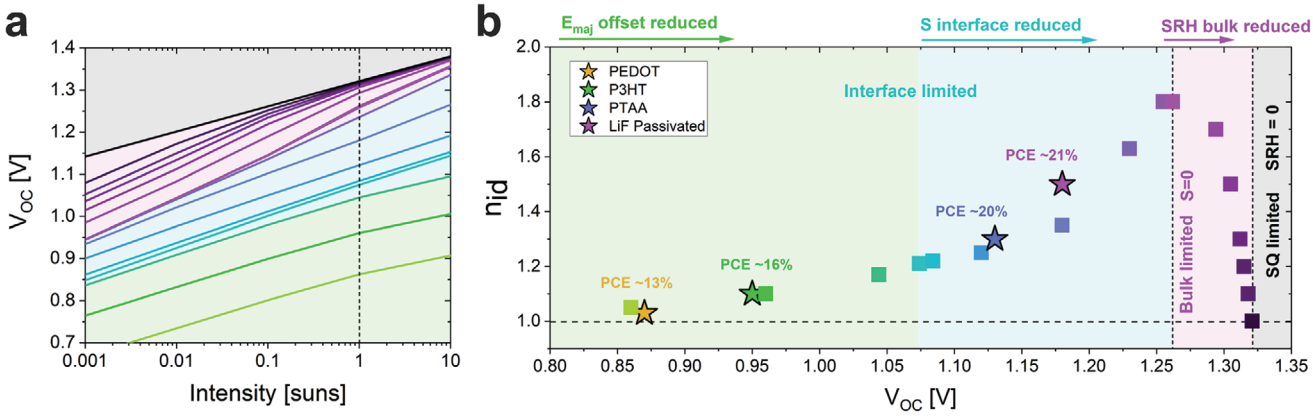

Figure 5. a) Numerically simulated intensity-dependent V_{OC} and b) external ideality factors at 1 sun of *p-i-n*-type perovskite cells as a function of V_{OC} by varying the interface recombination velocity *S* symmetrically at both interfaces from 1×10^5 to 0 (interface limited region) and subsequently the SRH recombination in the bulk (bulk limited region). The bulk SRH recombination has been reduced by increasing the bulk carrier lifetime from 400 ns to 10 µs. The black region represents the Shockley–Queisser (SQ) limit in the case of bimolecular recombination only. The stars indicate experimental V_{OC}s and n_{id} values for cells characterized by different degree of interface recombination and E_{maj} offsets. The cell with highest V_{OC} implement a interlayer of LiF at the C60 interface in order to reduce the effect of interfacial recombination.[13]

interface with strongly decreased V_{OC}. We succeeded in modeling a range of different n_{id} values, from 1 to 2, considering only first-order SRH recombination and the carrier densities (n_h and n_e) in the proximity of the dominant recombination channel. Essentially, these ideality factor values could be explained by an asymmetric shift of the electron/hole quasi-Fermi levels with increasing light intensity. This allowed us to explain the *mixed* ideality factor values typically observed in perovskite solar cells. Moreover, we rationalized that $n_{id} = 1$ does not always originate from predominant bimolecular recombination, but it can correspond to solar cells limited by interface recombination or recombination at the metal contacts in the case of a selectivity failure. In fact, by simulating interface or bulk recombination limited devices and correlating the results to the ideality factors of working devices, we showed that decreasing interface recombination increases simultaneously the V_{OC} and the n_{id}. In this picture, $n_{id} = 1$ may only be desirable if bulk recombination is dominating the total recombination in the cell. Overall, this work summarizes important aspects regarding the true meaning of the n_{id} values typically observed in perovskite solar cells and provides detailed insight into the underlying recombination processes in working devices.

4. Experimental Section

Device Preparation: Patterned indium tin oxide (ITO) (Lumtec, 15 Ω sqr.$^{-1}$) was washed with acetone, Hellmanex III, deionized-water, and isopropanol. After microwave plasma treatment (3 min at 200 W), PTAA (Sigma-Aldrich, M_n = 7000–10 000, polydispersity = 2–2.2) in a concentration of 1.5 mg mL^{-1} was spin coated at 6000 rpm for 30 s and immediately annealed for 10 min at 100 °C. After that, a 60 µL solution of poly(9,9-bis(3′-(*N*,*N*-dimethyl)-*N*-ethylammoinium-propyl-2,7-fluorene)-*alt*-2,7-(9,9-dioctylfluorene))dibromide (PFN-Br) (0.5 mg mL^{-1} in methanol) was added onto the spinning substrate at 5000 rpm for 20 s resulting in a film with a thickness below the detection limit of the atomic force microscopy (<5 nm). In the case of PEDOT:PSS as HTL, PEDOT:PSS (Heraeus Celivious 4083) was spin coated at 2000 rpm for 40 s (acceleration 2000 rpm s^{-1}) and subsequently annealed at 150 °C for 15 min. The perovskite layer was formed by spin coating a dimethyl formamide:dimethyl sulfoxide solution (4:1 volume) at 4500 rpm for 35 s. After 10 s of spin coating, 500 mL of diethyl ether (antisolvent) was dripped on top of the spinning substrate. After spin coating samples were annealed at 100 °C for 1 h. Afterwards, the samples were transferred to an evaporation chamber and C_{60} (30 nm), bathocuproine (8 nm) and copper (100 nm) were deposited under vacuum ($p = 10^{-7}$ mbar). The active area was 6 mm^2 defined as the overlap of ITO and the top electrode.

Current Density–Voltage Characteristics and EQE_{PV}: *JV*-curves were measured under N_2 with a Keithley 2400 system in a two-wire configuration with a scan speed of 0.1 V s^{-1} and voltage step of 0.02 V. One sun illumination at ≈100 mW cm^{-2} of AM1.5G irradiation was provided by a Oriel class ABA sun simulator. The real illumination intensity was monitored during the measurement using a Si photodiode and the exact illumination intensity was used for efficiency calculations. The sun simulator was calibrated with a KG5 filtered silicon solar cell (certified by Fraunhofer ISE). The AM1.5G short-circuit current of devices matched the integrated product of the external quantum efficiency (EQE) spectrum within 5–10% error. The latter was recorded using a home-built setup utilizing a Philips Projection Lamp (Type7724 12 V 100 W) in front of a monochromator (Oriel Cornerstone 74100) and the light was mechanically chopped at 70 Hz. The photogenerated current was measured using a lock-in-amplifier (EG&G Princeton Applied Research Model 5302, integration times 300 ms) and evaluated after calibrating the lamp spectrum with an UV-enhanced Si photodetector (calibrated at Newport).

Absolute Photoluminescence: Excitation for the PL measurements was performed with a 445 nm continuous wave laser (Insaneware) through an optical fibre into an integrating sphere. The intensity of the laser was adjusted to a 1 sun equivalent intensity by illuminating a 1 cm^2 size perovskite solar cell under short-circuit and matching the current density to the J_{SC} under the sun simulator (22.0 mA cm^{-2} at 100 mW cm^{-2}, or 1.375×10^{21} photons m^{-2} s^{-1}). A second optical fiber was used from the output of the integrating sphere to an Andor SR393i-B spectrometer equipped with a silicon charge-coupled device camera (DU420A-BR-DD, iDus). The system was calibrated by using a calibrated halogen lamp with specified spectral irradiance, which was shone into to integrating sphere. A spectral correction factor was established to match the spectral output of the detector to the calibrated spectral irradiance of the lamp. The spectral photon density was obtained from the corrected detector signal (spectral irradiance) by division through the photon energy (*hf*) and the photon numbers of the excitation and emission obtained from numerical integration using Matlab. In a last step, three fluorescent test samples with high specified PLQY (≈70%) supplied from Hamamatsu Photonics were measured where the specified value could be accurately reproduced within a small relative error of less than 5%

Measurement Conditions: All PL measurements were performed on complete cells, prepared fresh, and immediately encapsulated in a glovebox under N_2 atmosphere. The PL of the samples was readily recorded after mounting the sample and after an exposure of 1 s at each laser intensity subsequently, the incident laser was blocked by a shutter and the filter wheel position adjusted while the sample was kept in dark conditions avoiding any effects induced by constant illumination. The cell was illuminated through the glass/ITO side. It was noted that all absolute PL measurements were performed on films with the same HTL, ETL, and perovskite thicknesses as used in the operational solar cells.

Intensity Dependent V_{OC}: Intensity dependent V_{OC} measurements were performed illuminating the respective solar cell at exactly the same illumination condition and exposure time (1 s) as during the PL measurements in order to have the same experimental condition for the two measurements. To this end a mechanical shutter was used to illuminate the sample for 1 s for each given intensity. The corresponding V_{OC} was monitored with a Keithley 2400 system in a two-wire configuration.

Solar Cell Capacitance Simulator (SCAPS) Simulations: Simulation parameters and further details are discussed at Table S1 in the Supporting Information. SCAPS is an open-source code and can be obtained from the conditions requested by the developers Marc Burgelman and others.

Supporting Information

Supporting Information is available from the Wiley Online Library or from the author.

Acknowledgements

M.S. acknowledges the Deutsche Forschungsgemeinschaft (DFG, German Research Foundation)—Project No. 423749265—SPP 2196 (SURPRISE) for funding. S.A. acknowledges funding from the German Federal Ministry of Education and Research (BMBF), within the project "Materialforschung für die Energiewende" (Grant No. 03SF0540), and the German Federal Ministry for Economic Affairs and Energy (BMWi) through the "PersiST" project (Grant No. 0324037C). Additional funding came from HyPerCells (a Joint Graduate School of the Potsdam University and the Helmholtz-Zentrum Berlin) and by the DFG (German Research Foundation)—Project-ID 182087777—SFB 951. A.A. was supported by Sêr Cymru Program through the European Regional Development Fund, and Welsh European Funding Office.

Conflict of Interest

The authors declare no conflict of interest.

Keywords

device physics, ideality factor, perovskites, perovskite solar cells, solar cells

Received: February 7, 2020
Revised: April 27, 2020
Published online:

[1] G. Hodes, *Science* **2013**, *342*, 317.
[2] Q. Dong, Y. Fang, Y. Shao, P. Mulligan, J. Qiu, L. Cao, J. Huang, *Science* **2015**, *347*, 967.
[3] S. D. Stranks, G. E. Eperon, G. Grancini, C. Menelaou, M. J. P. Alcocer, T. Leijtens, L. M. Herz, A. Petrozza, H. J. Snaith, *Science* **2013**, *342*, 341.
[4] W.-J. Yin, T. Shi, Y. Yan, *Appl. Phys. Lett.* **2014**, *104*, 063903.
[5] M. Abdi-Jalebi, Z. Andaji-Garmaroudi, S. Cacovich, C. Stavrakas, B. Philippe, J. Richter, M. Alsari, E. P. Booker, E. Hutter, A. J. Pearson, S. Lilliu, T. J. Savenije, H. Rensmo, G. Divitini, C. Ducati, R. Friend, S. D. Stranks, *Nature* **2018**, *555*, 497.
[6] I. L. Braly, D. W. Dequilettes, L. M. Pazos-Outón, S. Burke, M. E. Ziffer, D. S. Ginger, H. W. Hillhouse, *Nat. Photonics* **2018**, *12*, 355.
[7] X. Zheng, B. Chen, J. Dai, Y. Fang, Y. Bai, Y. Lin, H. Wei, X. C. Zeng, J. Huang, *Nat. Energy* **2017**, *2*, 17102.
[8] W. S. Yang, B. Park, E. H. Jung, N. J. Jeon, Y. C. Kim, D. U. Lee, S. S. Shin, J. Seo, E. K. Kim, J. H. Noh, S. Il Seok, *Science* **2017**, *356*, 1376.
[9] T. S. Sherkar, C. Momblona, L. Gil-Escrig, J. Ávila, M. Sessolo, H. J. Bolink, L. J. A. Koster, *ACS Energy Lett.* **2017**, *2*, 1214.
[10] D. Bi, C. Yi, J. Luo, J.-D. Décoppet, F. Zhang, S. M. Zakeeruddin, X. Li, A. Hagfeldt, M. Grätzel, *Nat. Energy* **2016**, *1*, 16142.
[11] J.-P. Correa-Baena, W. Tress, K. Domanski, E. H. Anaraki, S.-H. Turren-Cruz, B. Roose, P. P. Boix, M. Grätzel, M. Saliba, A. Abate, A. Hagfeldt, *Energy Environ. Sci.* **2017**, *10*, 1207.
[12] K. Tvingstedt, L. Gil-Escrig, C. Momblona, P. Rieder, D. Kiermasch, M. Sessolo, A. Baumann, H. J. Bolink, V. Dyakonov, *ACS Energy Lett.* **2017**, *2*, 424.
[13] M. Stolterfoht, C. M. Wolff, J. A. Márquez, S. Zhang, C. J. Hages, D. Rothhardt, S. Albrecht, P. L. Burn, P. Meredith, T. Unold, D. Neher, *Nat. Energy* **2018**, *3*, 847.
[14] C. M. Wolff, P. Caprioglio, M. Stolterfoht, D. Neher, *Adv. Mater.* **2019**, *31*, 1902762.
[15] M. Stolterfoht, P. Caprioglio, C. M. Wolff, J. A. Márquez, J. Nordmann, S. Zhang, D. Rothhardt, U. Hörmann, Y. Amir, A. Redinger, L. Kegelmann, F. Zu, S. Albrecht, N. Koch, T. Kirchartz, M. Saliba, T. Unold, D. Neher, *Energy Environ. Sci.* **2019**, *12*, 2778.
[16] P. Caprioglio, M. Stolterfoht, C. M. Wolff, T. Unold, B. Rech, S. Albrecht, D. Neher, *Adv. Energy Mater.* **2019**, *9*, 1901631.
[17] V. Sarritzu, N. Sestu, D. Marongiu, X. Chang, S. Masi, A. Rizzo, S. Colella, F. Quochi, M. Saba, A. Mura, G. Bongiovanni, *Sci. Rep.* **2017**, *7*, 44629.
[18] P. Calado, D. Burkitt, J. Yao, J. Troughton, T. M. Watson, M. J. Carnie, A. M. Telford, B. C. O'Regan, J. Nelson, P. R. F. Barnes, *Phys. Rev. Appl.* **2019**, *11*, 044005.
[19] N. Wu, Y. Wu, D. Walter, H. Shen, T. Duong, D. Grant, C. Barugkin, X. Fu, J. Peng, T. White, K. Catchpole, K. Weber, *Energy Technol.* **2017**, *5*, 1827.
[20] W. Tress, *Adv. Energy Mater.* **2017**, *7*, 1602358.
[21] G. J. A. H. Wetzelaer, M. Scheepers, A. M. Sempere, C. Momblona, J. Ávila, H. J. Bolink, *Adv. Mater.* **2015**, *27*, 1837.
[22] W. Tress, M. Yavari, K. Domanski, P. Yadav, B. Niesen, J. P. Correa Baena, A. Hagfeldt, M. Graetzel, *Energy Environ. Sci.* **2018**, *11*, 151.
[23] T. Kirchartz, F. Deledalle, P. S. Tuladhar, J. R. Durrant, J. Nelson, *J. Phys. Chem. Lett.* **2013**, *4*, 2371.
[24] K. Tvingstedt, C. K. Deibel, *Adv. Energy Mater.* **2016**, *6*, 1502230.
[25] T. Kirchartz, B. E. Pieters, J. Kirkpatrick, U. Rau, J. Nelson, *Phys. Rev. B* **2011**, *83*, 115209.
[26] P. Würfel, *J. Phys. C Solid State Phys.* **1982**, *15*, 3967.
[27] S. Wheeler, D. Bryant, J. Troughton, T. Kirchartz, T. Watson, J. Nelson, J. R. Durrant, *J. Phys. Chem. C* **2017**, *121*, 13496.
[28] D. Kiermasch, L. Gil-Escrig, A. Baumann, H. J. Bolink, V. Dyakonov, K. Tvingstedt, *J. Mater. Chem. A* **2019**, *7*, 14712.
[29] O. Almora, K. T. Cho, S. Aghazada, I. Zimmermann, G. J. Matt, C. J. Brabec, M. K. Nazeeruddin, G. Garcia-Belmonte, *Nano Energy* **2018**, *48*, 63.
[30] T. Kirchartz, J. Nelson, *Phys. Rev. B* **2012**, *86*, 165201.
[31] K. Tvingstedt, L. Gil-Escrig, C. Momblona, P. Rieder, D. Kiermasch, M. Sessolo, A. Baumann, H. J. Bolink, V. Dyakonov, *ACS Energy Lett.* **2017**, *2*, 424.
[32] M. Saliba, T. Matsui, J.-Y. Seo, K. Domanski, J.-P. Correa-Baena, M. K. Nazeeruddin, S. M. Zakeeruddin, W. Tress, A. Abate, A. Hagfeldt, M. Grätzel, *Energy Environ. Sci.* **2016**, *9*, 1989.
[33] L. M. Pazos-Outón, T. P. Xiao, E. Yablonovitch, *J. Phys. Chem. Lett.* **2018**, *9*, 1703.
[34] R. Brenes, M. Laitz, J. Jean, D. W. DeQuilettes, V. Bulović, *Phys. Rev. Appl.* **2019**, *12*, 014017.
[35] D. W. deQuilettes, S. Koch, S. Burke, R. K. Paranji, A. J. Shropshire, M. E. Ziffer, D. S. Ginger, *ACS Energy Lett.* **2016**, *1*, 438.
[36] Y. Zhao, W. Zhou, W. Ma, S. Meng, H. Li, J. Wei, R. Fu, K. Liu, D. Yu, Q. Zhao, *ACS Energy Lett.* **2016**, *1*, 266.
[37] T. S. Sherkar, C. Momblona, L. Gil-Escrig, H. J. Bolink, L. J. A. Koster, *Adv. Energy Mater.* **2017**, *7*, 1602432.
[38] S. Wheeler, F. Deledalle, N. Tokmoldin, T. Kirchartz, J. Nelson, J. R. Durrant, *Phys. Rev. Appl.* **2015**, *4*, 024020.
[39] B. Dänekamp, N. Droseros, D. Tsokkou, V. Brehm, P. P. Boix, M. Sessolo, N. Banerji, H. J. Bolink, *J. Mater. Chem. C* **2019**, *7*, 523.
[40] T. Du, W. Xu, M. Daboczi, J. Kim, S. Xu, C.-T. Lin, H. Kang, K. Lee, M. J. Heeney, J.-S. Kim, J. R. Durrant, M. A. McLachlan, *J. Mater. Chem. A* **2019**, *7*, 18971.
[41] W. Xiang, Z. Wang, D. J. Kubicki, W. Tress, J. Luo, D. Prochowicz, S. Akin, L. Emsley, J. Zhou, G. Dietler, M. Grätzel, A. Hagfeldt, *Joule* **2019**, *3*, 205.